
This is an electronic reprint of the original article.
This reprint may differ from the original in pagination and typographic detail.

Ma, Xiaofeng; Särkkä, Simo

Indoor Positioning Methods Based on Dual Feet-Mounted IMUs With Distance Constraints

Published in:

Proceedings of the 2023 13th International Conference on Indoor Positioning and Indoor Navigation, IPIN 2023

DOI:

[10.1109/IPIN57070.2023.10332511](https://doi.org/10.1109/IPIN57070.2023.10332511)

Published: 01/01/2023

Document Version

Peer-reviewed accepted author manuscript, also known as Final accepted manuscript or Post-print

Please cite the original version:

Ma, X., & Särkkä, S. (2023). Indoor Positioning Methods Based on Dual Feet-Mounted IMUs With Distance Constraints. In *Proceedings of the 2023 13th International Conference on Indoor Positioning and Indoor Navigation, IPIN 2023* (International Conference on Indoor Positioning and Indoor Navigation). IEEE.
<https://doi.org/10.1109/IPIN57070.2023.10332511>

This material is protected by copyright and other intellectual property rights, and duplication or sale of all or part of any of the repository collections is not permitted, except that material may be duplicated by you for your research use or educational purposes in electronic or print form. You must obtain permission for any other use. Electronic or print copies may not be offered, whether for sale or otherwise to anyone who is not an authorised user.

Indoor Positioning Methods Based on Dual Feet-Mounted IMUs With Distance Constraints

Xiaofeng Ma[†]
Aalto University
Espoo, Finland
xiaofeng.ma@aalto.fi

Simo Särkkä
Aalto University
Espoo, Finland
simo.sarkka@aalto.fi

Abstract—The zero velocity update (ZUPT) offers an effective correction method for the sensor drift in indoor positioning systems using foot-mounted inertial measurement units (IMUs). However, the heading drift is still problematic in positioning systems using a single IMU. This paper studies methods for positioning using two foot-mounted IMUs. We propose two methods for this purpose, which are based on the use of a distance constraint and a spacing-vector constraint, respectively. Our methods are compared against other distance-constraint-based methods. The results reveal that our methods are able to achieve a better distribution concentration than the other methods, and they better control the separation between the trajectories of the feet.

Index Terms—indoor positioning, dual IMUs, foot-mounted, constraint

I. INTRODUCTION

Inertial navigation systems (INSs) are highly useful for positioning in environments where infrastructure-based positioning systems (e.g., GPS [1] and WiFi [2]) are not available. The accumulation of sensor errors makes INS unreliable for longer periods of time [3]. For pedestrian positioning, using a foot-mounted inertial measurement unit (IMU) is an effective solution to this problem because the periodic contacts of the foot with the ground provide pseudo-measurements that can be used to compensate for the sensor drifts. These pseudo-measurements can be used to make drift corrections which are called zero velocity updates (ZUPTs) [3]. However, the heading-related states are not observable from the zero velocity pseudo-measurements, which leads to a heading drift in the calculated trajectory. To reduce the drift, recent research has focused on the use of additional devices such as distance sensors, magnetometers integrated with the IMU, and fusion of multiple IMUs using physical constraints. We discuss these in the following.

As it is difficult to observe the heading-related states by relying only on the IMU itself, additional sensors can be used to provide reference measurements. For example, Xia et al. [4] use an ultrasonic sensor to detect changes in foot-to-wall distance to determine if there is a heading drift in the current calculated trajectory. However, adding more sensors like this may result in a bulky and cumbersome device.

[†] thanks financial support from the program of China Scholarships Council (CSC, No.202106020074) and the Academy of Finland.

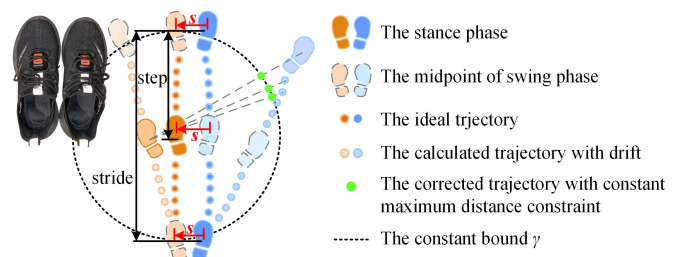


Fig. 1: Illustration of the concept of the paper. The trajectories of two feet calculated by independent INSs diverge due to a heading drift. We develop new methods to constrain them using the physical distance between the feet.

Magnetometers are also often used to obtain heading information as they can be integrated into an IMU. However, indoor environments may contain ferromagnetic substances that can interfere with geomagnetism [2]. One way to aid IMU-based positioning is to treat the disturbed magnetic field as a map of fingerprints [2]. To avoid the large effort of collecting a magnetic fingerprint map, Gaussian process regression can be used to estimate the magnetic field [5], [6]. Viset et al. [7] developed a method for simultaneous localisation and mapping of magnetic field using an extended Kalman filter (EKF). Nevertheless, Gaussian process regression methods for magnetic field-based positioning have difficulties in providing good predictions for unexplored areas.

Another kind of approach, which we also study here, is to place sensors on both feet. The drift can then be diminished by constraining the maximum distance between the feet [8]–[11]. In paper [8], the problem is formulated as an optimisation problem with an inequality constraint. Pratee et al. [9] give a closed-form solution for constraining the position of the swinging foot. Bolotin et al. [10] regard the maximum distance as a pseudo-observation for an EKF. Shi et al. [11] argues that an ellipsoidal boundary is more suitable than a spherical (distance) boundary because the height difference between the two feet in walking is more constrained than the horizontal distance.

The spherical and non-spherical constraint-based methods described above essentially pull the erroneous points beyond a threshold back onto the intersections of the boundary circle

with the lines joining the standing foot and those points. This is effective in correcting displacement errors in the forward direction. However, heading drift is often the main problem that makes the feet tracks diverge. Even when the lengths of the trajectories are calculated accurately, the wrong heading makes the feet tracks drift away from each other. This is illustrated in Fig. 1. As shown by the transparent dots in the figure, some points of the right foot are beyond the dashed circle. With the maximum distance constraint method, these points will be “corrected” to the green points, resulting in a loss of length.

In reality, the maximum distance constraint is rather loose because the distance between the feet varies from a maximum to a minimum and then increases again. Zhu et al. [12] and Qi et al. [13] take the real-time range measurement from two ultrasonic sensors mounted on each foot as observations for EKF. In paper [14], the minimum foot-to-foot distance, which is observed when the moving foot passes by the standing foot, is taken as a pseudo-measurement for EKF.

The use of two IMUs on a single foot is another research area in addition to the methods involving two IMUs on each foot. In reference [15], the joint equality constraint between the lateral side of the shoe and the calf is analysed and is used as an observation for EKF. In paper [16], two IMUs are mounted on the upper sides of the ankle and the toe, respectively. The geometry of the two placements during the swing and stance phases is analysed. The velocity and position relationships between the two are then used as observations for measurement updates.

Positioning using an array of IMUs is also possible and has turned out to have a good practical performance [17], [18]. It allows using statistical means to obtain better positioning results from the IMU array by cancelling out the noise. However, the cost, number of IMUs, and size of the module affect the accuracy and relative performance of the IMU array-based methods.

In this paper, we propose a distance constraint method based on [9] and further propose a novel spacing vector constraint method. For our experiments, we have collected our own datasets which are made publicly available. We compare the proposed methods with other methods using the datasets. The structure of the paper is the following. In Section II, we explain some of the terms related to walking movements that will be used throughout the text, and describe the implementation process of the ZUPT-only method which we use as a baseline. The proposed methods are explained in Section III. The collected datasets are explained and the methods are compared in Section IV. Finally, we conclude our work in Section V.

II. ZUPT-AIDED PEDESTRAIN POSITIONING

In this section, we define some terms related to walking and also define the single-foot model that is also used in the dual-foot case in the next section.

A. Gait cycle

Human walking is a periodic movement known as the gait cycle and a gait cycle can be divided into stance phase and

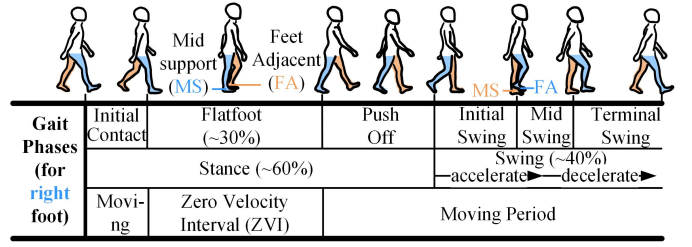


Fig. 2: Illustration of a gait cycle and important terms.

swing phase (see Fig. 2) [19], [20]. The period when ZUPT can be used is called the flatfoot phase which is also called the zero velocity interval (ZVI). In addition to the flatfoot phase, there are two short intervals at both ends of the stance phase. During these two phases, the foot is still supported on the ground, but it is rotating around the heel or toe and therefore ZUPT cannot be applied. We denote the remaining intervals of the gait cycle, except for the flatfoot period, collectively as the moving period. The midpoint of the flatfoot phase is called mid support (MS), at which the contralateral foot is right at the midpoint of its swing phase which is called feet adjacent (FA). The two feet are closest together when one foot is at MS and the other at FA.

We detect the ZVI by the generalised likelihood ratio test [3] and the moving period can therefore be determined because it is the complement of the ZVI in one stride. FA can be roughly detected by the maximum peak of the angular velocity in the horizontal axis of the human body [20].

B. Positioning with single foot-mounted IMU

Next, we describe the model often used in single foot-mounted IMUs which we also use in the dual-foot case. We estimate navigation the state $\mathbf{x}_k^{(i)}$ of i th system, which contains position $\mathbf{p}_k^{(i)}$, velocity $\mathbf{v}_k^{(i)}$, and quaternion $\mathbf{q}_k^{(i)}$, by EKF with the aid of ZUPT [8], [9], [21], [22].

The navigation equations are [22]:

$$\begin{bmatrix} \mathbf{p}_k^{(i)} \\ \mathbf{v}_k^{(i)} \\ \mathbf{q}_k^{(i)} \end{bmatrix} = \begin{bmatrix} \mathbf{p}_{k-1}^{(i)} + \mathbf{v}_{k-1}^{(i)} T_s \\ \mathbf{v}_{k-1}^{(i)} + T_s (C_b^n \mathbf{f}_k^{(i)} + \mathbf{g}^n - \mathbf{w}_k^{(i),a}) \\ \mathbf{q}_{k-1}^{(i)} \otimes \exp\left(\frac{T_s}{2} (\boldsymbol{\omega}_k^{(i)} - \mathbf{w}_k^{(i),g})\right) \end{bmatrix}, \quad (1)$$

where T_s is the sampling time, C_b^n is the rotation matrix from the body frame to the navigation frame, $\mathbf{f}_k^{(i)}$ is the specific force, $\mathbf{g}^n = [0 \ 0 \ -g]^\top$ is the gravity, $\boldsymbol{\omega}_k^{(i)}$ is the angular velocity, and $\mathbf{w}_k^{(i),a}$ and $\mathbf{w}_k^{(i),g}$ are Gaussian noises with zero means and covariances $\sigma_a^2 \mathbf{I}_3$ and $\sigma_g^2 \mathbf{I}_3$, respectively. Above, \otimes denotes the quaternion product and $\exp(\cdot)$ is the quaternion exponential. We assume the IMU is calibrated offline, so the sensor biases are not included in the system states.

The dynamics of error state are described as

$$\delta \mathbf{x}_k^{(i)} = \mathbf{F}_{k-1}^{(i)} \delta \mathbf{x}_{k-1}^{(i)} + \mathbf{G}_{k-1}^{(i)} \delta \mathbf{w}_{k-1}^{(i)}, \quad (2)$$

where $\delta \mathbf{x}_k^{(i)} = [\delta \mathbf{p}_k^{(i)\top} \ \delta \mathbf{v}_k^{(i)\top} \ \delta \boldsymbol{\theta}_k^{(i)\top}]^\top$ and $\delta \boldsymbol{\theta}_k$ is the error of the attitude. See the details of $\mathbf{F}_{k-1}^{(i)}$ and $\mathbf{G}_{k-1}^{(i)}$ in paper [8], [9], [21], [22].

Here we also take the static position as a pseudo-measurement in addition to the zero velocity, noted as $\mathbf{y}_k^{(i)} \triangleq [p_{x,k-1}^{(i)} \ p_{y,k-1}^{(i)} \ 0 \ 0 \ 0 \ 0]^\top$. Specifically, the xy -plane position (the first two elements of $\mathbf{y}_k^{(i)}$) should remain unchanged and the velocity (the last three elements of $\mathbf{y}_k^{(i)}$) should be zero during the stance phase. The height should also be zero during the stance phase since we only consider walking on flat indoor surfaces. The uncertainty of the pseudo-measurement can be regarded as Gaussian noise $\mathbf{r}_k^{(i)} \sim \mathcal{N}(\mathbf{0}, \mathbf{R}^{(i)})$, where $\mathbf{R}^{(i)}$ can be set to a suitable small value, for example, $\mathbf{R}^{(i)} = \text{diag}(0.01\mathbf{I}_3, 0.0001\mathbf{I}_3)$.

III. METHODS FOR POSITIONING WITH TWO FEET

In this section, we propose methods for the dual foot-mounted IMU case illustrated in Fig. 1. The first of the methods is a varying distance constraint (VDC) based method built on the constant maximum distance constraint (MaxDC) method discussed in [9]. After that, a spacing vector constraint (SVC) method is developed, which uses the vector representation of the separation of the two feet, resulting in a linear constraint.

A. Constant maximum distance constraint method

The maximum distance constraint (MaxDC) method solves the following optimisation problem with a nonlinear inequality constraint [9]:

$$\mathbf{p}_k = \arg \min_{\mathbf{p} \in \mathbb{R}^3} (\|\mathbf{p}_{\text{move},k} - \mathbf{p}\|_2^2), \text{ s.t. } \|\mathbf{p} - \mathbf{p}_{\text{MS}}\|_2^2 \leq \gamma^2, \quad (3)$$

where $\mathbf{p}_{\text{move},k}$ is the unconstrained position of the moving foot calculated via ZUPT, \mathbf{p}_{MS} is the position of the standing foot, and γ is the maximum distance bound.

The closed-form solution to the optimization problem obtained using the Lagrange multiplier method is [9]

$$\mathbf{p}_k = \mathbf{p}_{\text{MS}} + \frac{\gamma}{d_k} (\mathbf{p}_{\text{move},k} - \mathbf{p}_{\text{MS}}), \quad (4)$$

where $d_k = \|\mathbf{p}_{\text{move},k} - \mathbf{p}_{\text{MS}}\|$ is the distance between the standing foot and the unconstrained moving foot.

B. Proposed varying distance constraint method

As we explained in Section I, a constant distance constraint may not suffice for compensating the drifting of the two feet. Therefore, we develop the varying distance constraint (VDC) method, where the bound γ is allowed to be time-varying corresponding to the actual distance between the feet in each stride, that is, it is no longer just a constant. Below we use the notation γ_k for the time-varying bound.

The varying maximum distance constraint γ_k could be regarded as a simulated output of the ultrasound module in paper [12] and [13] during the moving period of each stride. As illustrated in Fig. 2, the moving period contains the swing phase, the initial contact phase, and the push-off phase. During the latter two phases, the displacement of the moving foot is very small since the foot is pivoting around the heel or toe. The distance of the two feet reaches the minimum at FA.

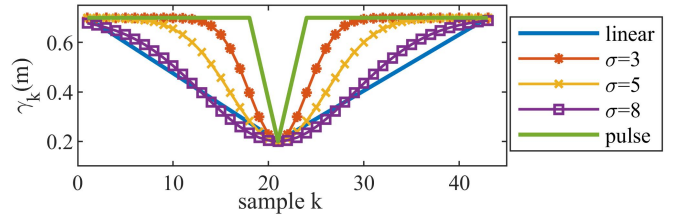


Fig. 3: Examples of candidates for time-varying bound γ_k . The blue line is just two straight lines connected, which only matches the minimum and maximum values without achieving a slow change at the ends and a smooth transition for the rest. The green line is another piece-wise linear function that can only correct points outside of the maximum boundary as well as at the FA point. The rest of the curves are flipped Gaussian density functions with different σ 's, and they more closely approximate the actual change in distance between the feet during one stride.

The displacement of the foot undergoes rapid changes during the remaining portion of the moving period, but mathematical modelling of this rapid change is harder.

Here we apply a simple model for γ_k curve which ensures that both ends of the moving period are sufficiently flat and vary smoothly toward an extreme value at FA. Several functions exhibit this characteristic shape, such as a vertically flipped Gaussian probability density function (see the curves labelled with different scale values in Fig. 3). For the experiments, we chose a flipped Gaussian with σ of 5.

Additionally, translation and scaling are necessary, when generating the γ_k curve, to ensure that

- the symmetry axis is located at FA of the current stride, and
- the minimum and maximum values are the set minimum and maximum distance between the two IMUs with a certain tolerance margin.

Using the bound γ_k in Fig. 3, thus induces an adaptive maximum distance constraint for each moment in a stride. Although our simulated pseudo-measurements are not as accurate as the real-time true measurements in papers [12] and [13], our method does not need the additional sensors, and avoids the corrections being concentrated at the end of a stride, thus eliminating the problems mentioned in Section I.

C. Proposed spacing vector constraint method

Due to physical constraints, the trajectories of the feet should not cross when a person walks. This is illustrated in Fig. 4, where the dark blue curve represents a reasonable trajectory for the right foot, while the light blue curve is considered unreasonable. Although the distance constraint method can limit the positions of the two IMUs to a reasonable range, it does not ensure that this physical requirement will be met. For this purpose, we propose the spacing vector constraint (SVC) method.

The spacing vector is the vector between two feet when the feet are side by side, see the red vector s in Fig. 1. Here

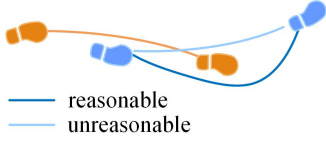


Fig. 4: Illustration of wrongly crossed foot tracks.

side by side means that the two feet are at the position closest to each other. This happens when one foot is at MS and the other at FA as described in Section II-A. The constraint in SVC applies only at these moments, such as the positions marked by three red s 's in Fig. 1. As the distance of the feet at these moments is quite stable for a fixed subject, it can be regarded as constant [14].

Assume that two IMUs are spaced $2a$ units apart when they are side by side, then we have

$$\begin{bmatrix} p_{R,x,k}^n \\ p_{R,y,k}^n \end{bmatrix} - \begin{bmatrix} p_{L,x,k}^n \\ p_{L,y,k}^n \end{bmatrix} = \mathbf{C}(\psi_k) \begin{bmatrix} 2a \\ 0 \end{bmatrix}, \quad (5)$$

where $p_{R,x,k}^n$ is the x -axis coordinate of the right (R) foot, and the subscript L indicates the left foot. Above,

$$\mathbf{C}(\psi_k) = \begin{bmatrix} \cos \psi_k & -\sin \psi_k \\ \sin \psi_k & \cos \psi_k \end{bmatrix}, \quad (6)$$

where ψ_k is the heading of the person. Here we simply take the circular average of the two heading angles of the two IMU as ψ_k :

$$\psi_k = \arctan \frac{\sin \psi_{R,k} + \sin \psi_{L,k}}{\cos \psi_{R,k} + \cos \psi_{L,k}}, \quad (7)$$

where $\psi_{R,k}$ and $\psi_{L,k}$ can be calculated from the quaternions of the right foot and left foot, respectively.

Substituting (7) into (5), we get

$$\begin{aligned} & \begin{bmatrix} p_{R,x,k}^n \\ p_{R,y,k}^n \end{bmatrix} - \begin{bmatrix} p_{L,x,k}^n \\ p_{L,y,k}^n \end{bmatrix} \\ &= \begin{bmatrix} 2a(\sin \psi_{R,k} + \sin \psi_{L,k}) \\ \sqrt{(\sin \psi_{R,k} + \sin \psi_{L,k})^2 + (\cos \psi_{R,k} + \cos \psi_{L,k})^2} \\ 2a(\cos \psi_{R,k} + \cos \psi_{L,k}) \\ \sqrt{(\sin \psi_{R,k} + \sin \psi_{L,k})^2 + (\cos \psi_{R,k} + \cos \psi_{L,k})^2} \end{bmatrix}. \end{aligned} \quad (8)$$

If we define $\mathbf{x}_c = [p_{R,x,k}^n \ p_{R,y,k}^n \ p_{L,x,k}^n \ p_{L,y,k}^n]^\top$, then (8) can be written as

$$\mathbf{D}\mathbf{x}_c = \mathbf{d}, \quad (9)$$

where $\mathbf{D} = [\mathbf{I}_2 \ -\mathbf{I}_2]$, and \mathbf{d} is the right hand side of (8). We use the estimate projection method [23] to implement this constraint on MS and FA positions of the two feet.

IV. EXPERIMENTAL RESULTS

In this section we describe our experimental datasets and also report the results of comparing the proposed methods to alternative methods.

A. Experimental setup and data collection

We used two Xsens DOT sensors to collect movement data. The two IMUs were placed as shown in Fig. 1. The data from the two IMUs was sampled at 60Hz and sent to a mobile phone via Bluetooth. As the ground truth, we used markers taped on the ground as a reference due to the lack of a high-accuracy reference system. We marked the ground at regular intervals (1.2m) for one foot, and the markings enclose a rectangle. The subject stepped on these markers in a predetermined order. The 1.2 meters is the normal stride length of the subject in this experiment.

In this paper, 30 sets of measurements collected under the same conditions were used. For each measurement set, the subject first stood for approximately 5 seconds to obtain the data used to calculate the initial pitch, roll, and gyroscope bias. Then the subject walked counterclockwise along the rectangle with the right foot stepping on the markers, that is, one step length is approximately 0.6m. To evaluate the performance over longer distances, we extended each measurement by repeating it four times as in [22].

In addition, we also collected measurements in other situations done by another subject, walking clockwise, around an 8-shaped path, and around a running track. Due to space limitations, in this paper, we only evaluate the methods on datasets done by one subject walking counterclockwise along the rectangle. All data sets are publicly available¹.

B. Initial heading alignment

Some studies of 6DOF-IMU-based positioning methods have overlooked the importance of properly setting the initial heading. In some cases, the forward axis of the sensor may not be strictly aligned with zero heading at the beginning, which results in a non-zero real heading angle. This may lead to a heading error that outweighs the drift caused by the gyroscope errors. Here, we take the heading calculated by the two MS positions at the start and end of the first stride for both left and right foot respectively as the initial direction of each foot.

C. Comparison of the methods

We compared our methods (VDC and SVC) with ZUPT, MaxDC [9], and the minimum distance constraint method (MinDC) [14] which takes minimum distance as a constraint at MS-FA. The resulting trajectories of the five methods of a particular walking are shown in Figs. 5 and 6. The walking sequence starts from the triangles along the positive y -axis and then counter-clockwise along the windmill back to the triangles (see the black arrows in the figures).

The ZUPT-only approach results in increasing drift and widening separation between the trajectories of the two feet. The other four methods are capable of reducing this gap. From the small windows of zoomed-in details, only SVC guarantees the fact that the right foot is on the right and the left foot is on the left when the true forward direction is shown by the black arrow. The trajectories calculated by the other methods swap

¹https://github.com/xf-ma/dual-feet_datasets

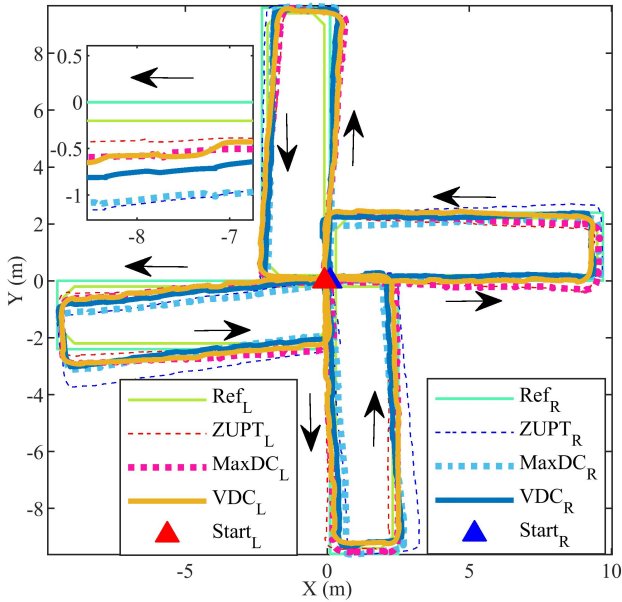


Fig. 5: Results of ZUPT along with maximum distance constraint (MaxDC) and varying distance constraint (VDC) methods.

left and right after an incorrect trajectory crossover occurs. However, none of them can essentially correct the heading state, and therefore the overall direction of the trajectories won't be better than the best of the two ZUPT results.

To investigate the distributions of the position estimates over different datasets, we applied the five methods to them and took the coordinates at MS of the 68th stride of the left and right footsteps, respectively. The results are displayed in Fig. 7. The true 2D coordinate of the right foot is $(-8.3\text{m}, 0.0\text{m})$ and that of the left foot is about $(-7.7\text{m}, -0.2\text{m})$.

Fig. 7 shows that the results from ZUPT exhibit dispersed distributions. The MaxDC and MinDC methods introduce a larger uncertainty in the forward direction (stride 68 forward direction is towards the negative x -axis), as is evident from the larger distribution span along the x -axis. And the distributions of VDC and SVC are generally more concentrated, especially in terms of forward direction. The SVC method displays the most concentrated distribution among the four constraining methods.

We have explained the limitation of the maximum distance constraint in Section I. Here we show an experimental example of a significant error caused by it in Fig. 8. Specifically, the distance between the left and right feet exceeded the threshold at point A, at which juncture the right foot was in the stance phase (depicted by the yellow circle). Before point A, the left foot was moving upwards from the bottom, and the distance between the two feet was within the constraint. Due to a heading error, the next trajectory point of the left foot after point A slopes downwards to the left, and the points beyond the bound are erroneously “corrected” to the purple arc that is connected by AB. This leads to a serious distortion of the

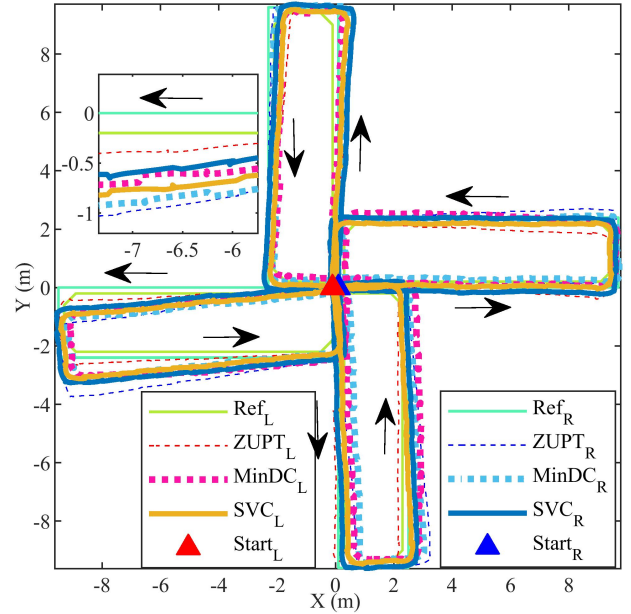


Fig. 6: Results of ZUPT along with minimum distance constraint (MinDC) and spacing vector constraint (SVC) methods.

TABLE I: The difference between the means of the coordinates of the feet (in meters).

	ZUPT	MaxDC	VDC	MinDC	SVC	True
$y_R - y_L$	0.50	-0.03	-0.12	-0.05	0.09	0.20
$x_R - x_{R, True}$	0.07	0.41	0.32	0.30	0.16	0.00
$x_L - x_{L, True}$	0.23	0.41	0.30	0.32	0.20	0.00

trajectory.

The mean values of the coordinates for the different methods are compared in Table I. The constraint methods are all able to constrain the trajectory spacing to some extent, of which the results of VDC and SVC methods are closer to the true value. The mean values of the coordinate estimates for the forward direction (x -axis) of the SVC are also very close to the true value, while the estimates for this from the other constraint methods differ from the true value larger. In summary, the performance of SVC is slightly better in this experiment.

The performance of the methods may be affected by the detection of FA and MS. Here, we detect FAs by gyroscope peaks as described in section II-A, and take ZVI midpoint as MS. This works for most people, but the threshold parameters in the detection algorithm of ZVI and FA may need to be fine-tuned due to different individuals and different IMU placements. Therefore, a more robust gait key event detection method can improve the robustness of our methods.

V. CONCLUSION

In this paper, we have proposed positioning methods based on distance constraint and spacing vector constraint (VDC and SVC), and compared them with other similar methods (MaxDC and MinDC). Our methods are better in representing

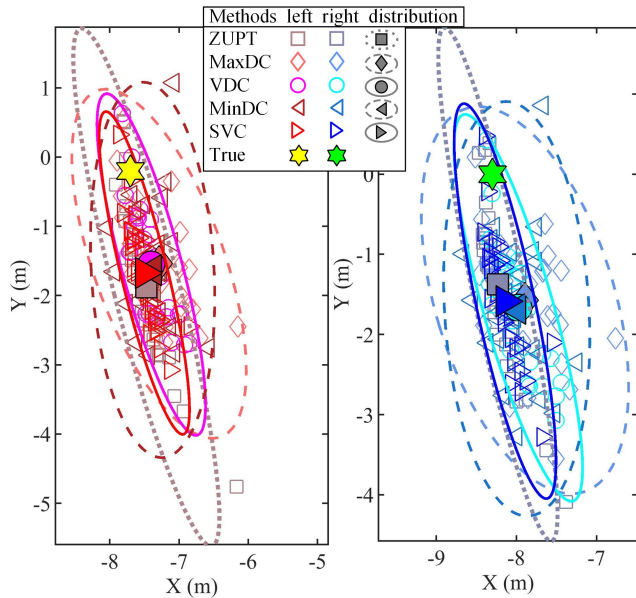


Fig. 7: The positions and distributions of 68th strides of the two feet calculated with different methods. The results of the different methods are shown as hollow symbols of different shapes and different colours, where the reddish ones are left-foot related and the bluish ones are right-foot related. The corresponding distributions are represented as solid black-edged symbols (means) and ellipses (covariances), of which the ellipses with solid edges are the proposed methods.

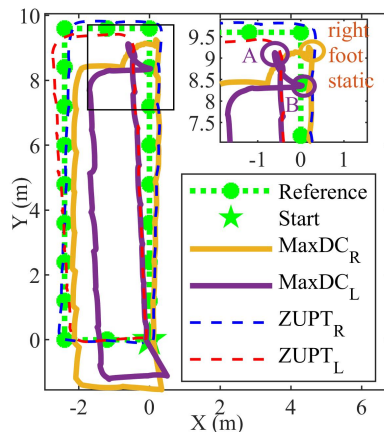


Fig. 8: An example of a spherical bound constraint problem.

the uncertainty of the results over multiple data sets and in constraining the spacing between the feet. However, all of these methods fall short in addressing the issue of overall heading drift optimally. They are suboptimal and will not improve the accuracy of the attitude estimate, since they do not take into account the uncertainty in the position estimate and the correlation between the position state and the other states. In the future, we will continue to improve our approaches in terms of more accurate physical modelling, leveraging of the physical constraints even better, and evaluating the methods

on more subjects and more path shapes.

REFERENCES

- [1] M. S. Grewal, L. R. Weill, and A. P. Andrews, *Global Positioning Systems, Inertial Navigation, and Integration*. John Wiley & Sons, 2007.
- [2] N. Samama, *Indoor Positioning: Technologies and Performance*. Hoboken, New Jersey: John Wiley & Sons, Inc, 2019.
- [3] J. Wahlstrom and I. Skog, "Fifteen years of progress at zero velocity: A review," *IEEE Sensors J.*, vol. 21, pp. 1139–1151, Jan. 2021.
- [4] M. Xia, C. Xiu, D. Yang, and L. Wang, "Performance enhancement of pedestrian navigation systems based on low-cost foot-mounted MEMS-IMU/ultrasonic sensor," *Sensors*, vol. 19, no. 2, 2019.
- [5] N. Akai and K. Ozaki, "Gaussian processes for magnetic map-based localization in large-scale indoor environments," in *2015 IEEE/RSJ International Conference on Intelligent Robots and Systems (IROS)*, (Hamburg, Germany), pp. 4459–4464, IEEE, Sept. 2015.
- [6] A. Solin, M. Kok, N. Wahlström, T. B. Schön, and S. Särkkä, "Modeling and interpolation of the ambient magnetic field by Gaussian processes," *IEEE Transactions on robotics*, vol. 34, no. 4, pp. 1112–1127, 2018.
- [7] F. Viset, R. Helmons, and M. Kok, "An extended Kalman filter for magnetic field SLAM using Gaussian process regression," *Sensors*, vol. 22, no. 8, p. 2833, 2022.
- [8] I. Skog, J.-O. Nilsson, D. Zachariah, and P. Händel, "Fusing the information from two navigation systems using an upper bound on their maximum spatial separation," in *2012 International Conference on Indoor Positioning and Indoor Navigation (IPIN)*, pp. 1–5, 2012.
- [9] G. Prateek, R. Girisha, K. Hari, and P. Händel, "Data fusion of dual foot-mounted INS to reduce the systematic heading drift," in *4th International Conference on Intelligent Systems, Modelling and Simulation*, pp. 208–213, 2013.
- [10] Y. Bolotin, A. Bragin, and D. Gulevskiy, "On consistency of EKF for pedestrian dead reckoning with foot mounted IMU," in *27th Saint Petersburg International Conference on Integrated Navigation Systems (ICINS)*, pp. 1–10, 2020.
- [11] W. Shi, Y. Wang, and Y. Wu, "Dual MIMU pedestrian navigation by inequality constraint Kalman filtering," *Sensors*, vol. 17, no. 2, 2017.
- [12] M. Zhu, Y. Wu, and S. Luo, "PIMU-R: Pedestrian navigation by low-cost foot-mounted dual IMUs and interfoot ranging," *IEEE Trans. Contr. Syst. Technol.*, vol. 30, no. 1, pp. 247–260, 2022.
- [13] L. Qi, Y. Yu, Y. Liu, C. Gao, T. Feng, J. Hui, and S. Wang, "A robust foot-mounted positioning system based on dual IMU data and ultrasonic ranging," *IEEE Sensors J.*, pp. 1–1, 2023.
- [14] X. Niu, Y. Li, J. Kuang, and P. Zhang, "Data fusion of dual foot-mounted IMU for pedestrian navigation," *IEEE Sensors J.*, vol. 19, no. 12, pp. 4577–4584, 2019.
- [15] H. Ju, J. H. Lee, and C. G. Park, "Pedestrian dead reckoning system using dual IMU to consider heel strike impact," in *18th International Conference on Control, Automation and Systems (ICCAS)*, pp. 1307–1309, 2018.
- [16] Z. Li, X. Xu, M. Ji, J. Wang, and J. Wang, "Pedestrian positioning based on dual inertial sensors and foot geometric constraints," *IEEE Trans. Ind. Electron.*, vol. 69, no. 6, pp. 6401–6409, 2022.
- [17] L. Xing, X. Tu, and Z. Chen, "Foot-mounted pedestrian navigation method by comparing ADR and modified ZUPT based on MEMS IMU array," *Sensors*, vol. 20, no. 13, 2020.
- [18] L. Wang, H. Tang, T. Zhang, Q. Chen, J. Shi, and X. Niu, "Improving the navigation performance of the MEMS IMU array by precise calibration," *IEEE Sensors J.*, vol. 21, no. 22, pp. 26050–26058, 2021.
- [19] A. Kharb, V. Saini, Y. K. Jain, and S. Dhiman, "A review of gait cycle and its parameters," 2011.
- [20] J. C. Pérez-Ibarra, A. A. G. Siqueira, and H. I. Krebs, "Real-time identification of gait events in impaired subjects using a single-imu foot-mounted device," *IEEE Sensors Journal*, vol. 20, no. 5, pp. 2616–2624, 2020.
- [21] E. Foxlin, "Pedestrian tracking with shoe-mounted inertial sensors," *IEEE Comput. Grap. Appl.*, vol. 25, pp. 38–46, Nov. 2005.
- [22] M. Kok, F. Viset, and M. Osman, "A framework for indoor localization using the magnetic field," in *2022 23rd IEEE International Conference on Mobile Data Management (MDM)*, pp. 385–387, 2022.
- [23] D. Simon, "Kalman filtering with state constraints: a survey of linear and nonlinear algorithms," *IET Control Theory & Applications*, vol. 4, pp. 1303–1318, Aug. 2010.